

R-Configuration of 4-Aminopyridyl-Based Inhibitors of CYP51 Confers Superior Efficacy Against *Trypanosoma cruzi*

Jun Yong Choi,[†] Claudia M. Calvet,^{‡,§,||} Debora F. Vieira,^{‡,§} Shamila S. Gunatilleke,^{‡,§,#} Michael D. Cameron,[‡] James H. McKerrow,^{‡,§} Larissa M. Podust,^{*,‡,§} and William R. Roush^{*,†}

[†]Department of Chemistry, Scripps Florida, Jupiter, Florida 33458, United States

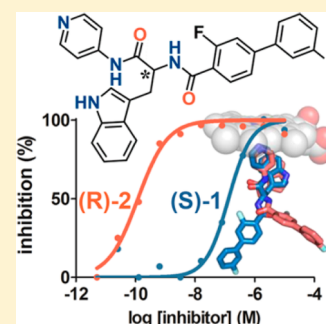
[‡]Center for Discovery and Innovation in Parasitic Diseases and [§]Department of Pathology, University of California San Francisco, San Francisco, California 94158, United States

^{||}Cellular Ultra-Structure Laboratory, Oswaldo Cruz Institute (IOC), FIOCRUZ, Rio de Janeiro, RJ 21040-362, Brazil

[‡]Department of Molecular Therapeutics, Scripps Florida, Jupiter, Florida 33458, United States

S Supporting Information

ABSTRACT: Sterol 14 α -demethylase (CYP51) is an important therapeutic target for fungal and parasitic infections due to its key role in the biosynthesis of ergosterol, an essential component of the cell membranes of these pathogenic organisms. We report the development of potent and selective D-tryptophan-derived inhibitors of *T. cruzi* CYP51. Structural information obtained from the cocrystal structure of CYP51 and (R)-2, which is >1000-fold more potent than its enantiomer (S)-1, was used to guide design of additional analogues. The in vitro efficacy data presented here for (R)-2–(R)-8, together with preliminary in vitro pharmacokinetic data suggest that this new CYP51 inhibitor scaffold series has potential to deliver drug candidates for treatment of *T. cruzi* infections.



KEYWORDS: *T. cruzi*, CYP51, R-configuration, inhibitors

The sterol biosynthesis pathway has been identified as an important therapeutic target for antifungal agents due to the different set of sterols that occur in fungal membranes as opposed to mammalian cell membranes.^{1,2} Sterol 14 α -demethylase (CYP51) catalyzes the oxidative removal of the 14-methyl group of lanosterol. The resulting $\Delta^{14,15}$ -unsaturated intermediate is subsequently converted to ergosterol, an essential fungal cell membrane component. CYP51 is also a potential chemotherapeutic target for the treatment of infection by the protozoan parasite *Trypanosoma cruzi* because *T. cruzi*'s membrane sterol components are similar to those of fungi, and the organism utilizes an analogous pathway for ergosterol biosynthesis.³ Thus, antifungal azole drugs have been repurposed as antiparasitic agents for treatment of Chagas disease.^{4–8} These agents, as well as the new *T. cruzi* CYP51 inhibitors tipifarnib, NEU321, and VNI analogues utilize azoles as a heme-binding unit. Consequently, resistance is a potential issue since resistance to azole drugs in cell culture and in *T. cruzi* infected mice has been reported.⁹ Consequently, an important objective for development of drugs to treat *T. cruzi* infection is to identify potent and safe CYP51 inhibitors based on nonazole chemotypes.

In this letter we describe the structure-guided development of a series of potent and selective N-indolyl-oxopyridinyl-4-aminopropanyl D-tryptophan-derived inhibitors of *T. cruzi* CYP51 that utilize a pyridine ring to coordinate to the heme group. The binding pose of the R-enantiomer of one of these

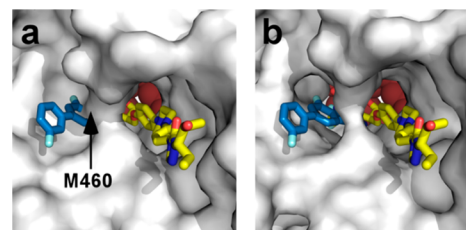


Figure 1. Comparison of the binding modes of (S)-1 (blue) and posaconazole (yellow) in the active site of *T. brucei* CYP51. Protein is shown as solvent accessible surface with the M460 side chain present in 2X2N (a) or omitted (b) from the 4BJK coordinates.

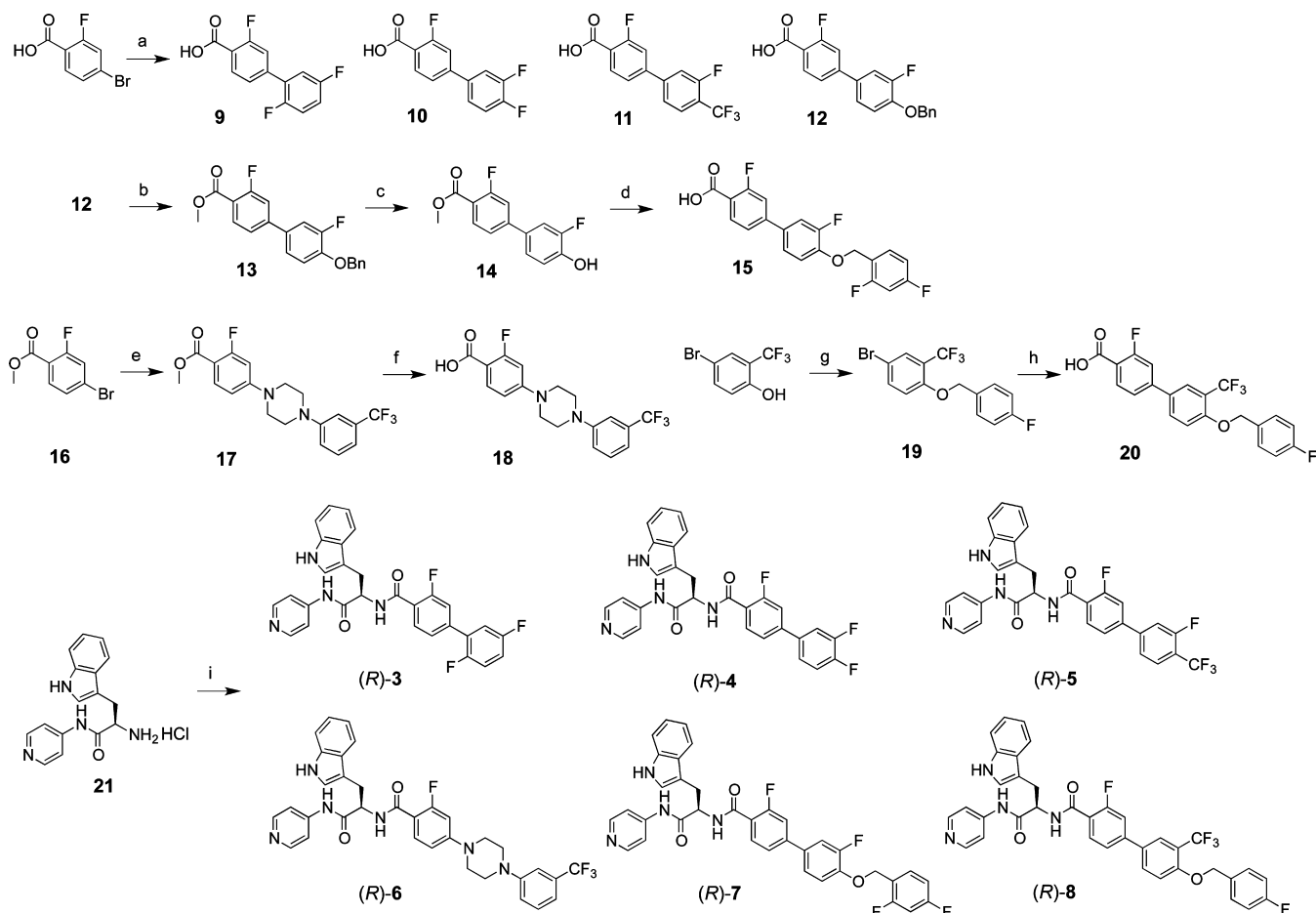
new inhibitors ((R)-2, derived from D-tryptophan) in the cocrystal structure with *T. cruzi* CYP51 is quite different from that of its S-enantiomer ((S)-1, derived from L-tryptophan).¹⁰ Relationships between the binding poses and inhibitory potential toward *T. cruzi* are presented and analyzed herein.

The nonazole CYP51 inhibitor LP10, which was initially identified by HTS,¹¹ possesses moderate inhibition potency (EC_{50} = 680 nM) against *T. cruzi* in infected mammalian cells. However, its closely related analogues have poor stability in liver microsome preparations ($t_{1/2}$ = <7 min) and poor

Received: January 9, 2014

Accepted: January 15, 2014

Published: January 22, 2014

Scheme 1. Synthesis of Key Intermediates **9**, **10**, **11**, **15**, **18**, and **20** and Inhibitors (*R*)-**3**–(*R*)-**8**^a

^aReagents and conditions: (a) arylboronic acid, 5 mol % Pd₂(dba)₃, 10 mol % PCy₃, 2 M K₃PO₄, dioxane, 100 °C (microwave), 1 h, ca. 90%; (b) H₂SO₄/MeOH (1/10), 70 °C, 24 h, 91%; (c) H₂ (balloon), Pd/C, MeOH–acetone, 23 °C, 24 h, 92%; (d) 2,4-difluorobenzyl bromide, K₂CO₃, acetone, 70 °C, 5 h, 95%; (e) 1-(3-(trifluoromethyl)phenyl)piperazine, Pd(OAc)₂, P(*o*-tolyl)₃, Cs₂CO₃, toluene, 50 °C, 48 h, 88%; (f) 10% NaOH (aq), MeOH, THF, 70 °C, 2 h, 99%; (g) 4-fluorobenzyl bromide, K₂CO₃, acetone, 50 °C, 12 h, 91%; (h) 4-carboxy-3-fluorophenylboronic acid, 5 mol % Pd₂(dba)₃, 10 mol % PCy₃, 2 M K₃PO₄, dioxane, 110 °C (microwave), 1 h, 30%; (i) **9**, **10**, **11**, **15**, **18**, or **20** (as appropriate), PyBOP, HOBT, Et₃N, CH₂Cl₂, 23 °C, 1 h, ca. 70%.

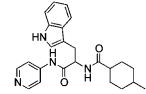
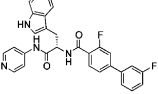
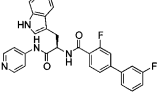
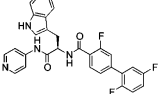
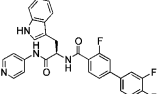
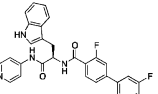
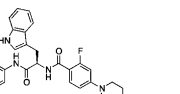
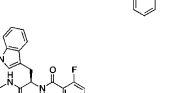
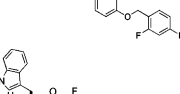
selectivity against human metabolic cytochrome P450 (CYP) enzymes (92, 77, and 75% inhibition of CYPs 2C9, 2D6, and 3A4 at 1 μM, respectively).¹⁰ Despite LP10s suboptimal pharmacokinetic properties, its promising efficacy in an animal model of acute *T. cruzi* infection⁷ encouraged to pursue structure-aided hit-to-lead optimization studies.

We recently reported results of first generation structure-based optimization of LP10.¹⁰ Initially, the *S*-enantiomers of LP10 analogues (deriving from *L*-tryptophan) were pursued because of better binding affinity and inhibitor potency compared to those with *R*-configuration at the tryptophan center. However, in spite of considerable effort, we were unable to identify CYP51 inhibitors with EC₅₀s less than 10 nM.⁵ During the course of these studies the X-ray cocrystal structure of the biaryl inhibitor (*S*)-**1** complexed with *T. brucei* CYP51 was determined to a resolution of 2.7 Å.⁵ From an in-depth comparison of the binding modes of (*S*)-**1** and posaconazole in the active site of CYP51,^{10,12} we identified several critical features that we used in the design of the next generation of substantially improved CYP51 inhibitors that we report herein. Specifically, although the biaryl unit of (*S*)-**1** and the tail portion of posaconazole are oriented toward a solvent-

accessible area, they protrude through different hydrophobic tunnels (Figure 1). The ample void space surrounding the biaryl unit of (*S*)-**1** and the tail unit of posaconazole suggested the possibility that the (*R*)-enantiomer of (*S*)-**1**, specifically inhibitor (*R*)-**2**, could adopt a different binding orientation compared to (*S*)-**1**.

To test this assumption, (*R*)-**2** and a series of additional analogues were synthesized starting from *D*-tryptophan, using the general procedure used previously for (*S*)-**1** (Scheme 1).¹⁰ Briefly, 4-bromo-2-fluorobenzoic acid was subjected to palladium-mediated coupling reactions^{13–16} with various aryl boronic acids to provide biaryl intermediates such as **9**, **10**, **11**, and **12**. Carboxylic acid **12** was converted to methyl ester **13**, and then the benzyl group was replaced with a 2,4-difluorobenzyl unit through catalytic hydrogenation (Pd/C and H₂) followed by O-alkylation with 2,4-difluorobenzyl bromide. Pd(0)-mediated coupling^{17–19} of *N*-aryl piperazine with **16** provided **17**, which was then hydrolyzed to give carboxylic acid **18**. O-alkylation of commercially available 4-bromo-2-(trifluoromethyl)phenol with 4-fluorobenzyl bromide followed by Suzuki coupling with 4-carboxy-3-fluorophenylboronic acid generated carboxylic acid **20**. All carboxylic acid

Table 1. Efficacy, Microsome Stability, and CYP Inhibition Profile of New Key CYP51 Inhibitors

Cpd	Structure	EC ₅₀ , (nM) ^a	Microsome Stability ^b			%inhibition of human CYPs ^c at 1 μM			
			t _{1/2} (min)	h	r	m	1A2	2C9	2D6
LP10		680 ^d	-	-	-	-	-	-	-
(S)-1 ^e		130±70 ^e	17	25	36	31	85	54	73
(R)-2		0.12±0.04	18	20	27	14	91	30	60
(R)-3		1.3±1.0	17	17	22	3	92	47	74
(R)-4		0.017±0.007	18	22	39	-21	90	48	48
(R)-5		2.9±0.3	45	39	69	-4	92	27	24
(R)-6		0.47±0.15	8	24	11	10	96	74	86
(R)-7		0.60±0.16	25	30	34	-9	84	21	38
(R)-8		9.2±5.2	29	53	51	-26	41	-17	15

^aEC₅₀ of compounds as determined vs. *T. cruzi*-infected mouse C2C12 myoblasts (see Supporting Information for details and Figure S1 for dose–response curves). EC₅₀ values were used to assess inhibitor potency since the UV–vis CYP51 binding assay is incapable of discriminating between compounds with IC₅₀ < 10 nM (ref 10). ^bStability of compounds in human (h), rat (r), and mouse (m) liver microsomes as evaluated in comparison to the Sunitinib reference (see Supporting Information). ^cInhibition of CYPs as evaluated in human liver microsomes using selective marker substrates for each CYP (see Supporting Information). ^dReported previously (ref 11). ^eReported previously (ref 10).

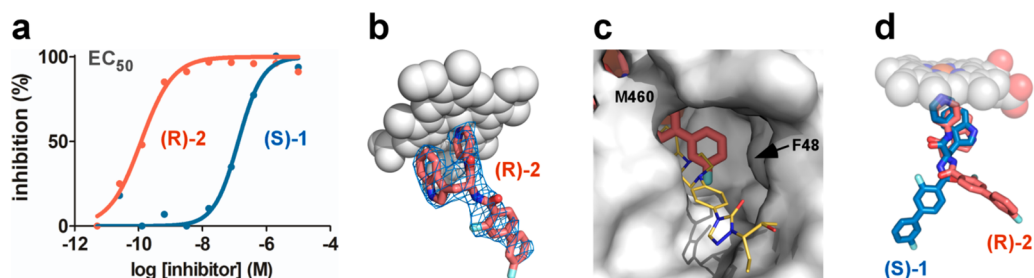


Figure 2. Binding and anti-*T. cruzi* activity of (S)-1 and (R)-2. (a) Dose–response curves for (S)-1 (blue) and (R)-2 (red) show >1000-fold difference in potency (*T. cruzi* cell-based assay). (b) A fragment of the 2F_o – F_c electron density map (blue mesh) contoured at $\sigma = 1.0$ corresponds to (R)-2 (red). Heme is shown in gray spheres. (c) (R)-2 viewed through the opening of the hydrophobic tunnel in 4BY0. Protein is represented by solvent accessible surface. Binding pose of posaconazole (yellow sticks) is derived from the superimposed 2X2N structure. (d) Overlap between (S)-1 (blue) and (R)-2 (red) derived from the superimposed structures, 4BJK and 4BY0, respectively. Heme is shown in semitransparent spheres.

intermediates were coupled with D-tryptophan derivative **21**⁵ to provide the final compounds **3–8**.²⁰

As shown in Table 1 and Figure 2A, the potency of (*R*)-**2** as an inhibitor of *T. cruzi* in infected cells increased >1000-fold compared to (*S*)-**1**, making (*R*)-**2** the first pM inhibitor derived from LP10. The new inhibitor (*R*)-**2** retained good microsomes stability and had an acceptable profile for inhibition of human CYPs.

The X-ray cocrystal structure of (*R*)-**2** with *T. cruzi* CYP51 was determined to a resolution of 3.1 Å (PDB ID 4BY0) (See Supporting Information for details). The diffraction data and refinement statistics are shown in Table 2. Despite a relatively

Table 2. X-ray Data Collection and Refinement Statistics

protein	<i>T. cruzi</i> CYP51
inhibitor	(<i>R</i>)- 2 (small molecule code SPS)
PDB ID	4BY0
Data Collection	
space group	P3 ₂ 21
cell dimensions	
<i>a</i> , <i>b</i> , <i>c</i> (Å)	124.2, 124.2, 119.8
α , β , γ (deg)	90.0, 120, 90.0
molecules in AU	2
wavelength	1.11587
resolution (Å)	3.10
R_{sym} or R_{merge} (%)	15.6 (134.3) ^a
$I/\sigma I$	9.6 (1.5)
completeness (%)	100.0 (100.0)
redundancy	8.2 (8.4)
Crystallization Conditions	
	0.2 M ammonium sulfate
	0.1 M Bis-Tris
	pH 6.5
	25% PEG 3350
Refinement	
no. reflections	18756
$R_{\text{work}}/R_{\text{free}}$ (%)	23.2/29.7
no. atoms	
protein	6663
heme	86
ligand	74
solvent	13
mean B value	78.2
B-factors	
protein	81.4
heme	62.0
ligand	72.0
solvent	52.1
rmsd	
bond lengths (Å)	0.011
bond angles (deg)	1.664

^aValues in parentheses are for highest resolution.

low resolution, electron density unambiguously defined (*R*)-**2** in the active site (Figure 2B), indicating that the biaryl unit of (*R*)-**2** is oriented toward the hydrophobic tunnel that is utilized by the tail of posaconazole (Figure 2C). (*R*)-**2** is distinguished by an L-shape in the active site of *T. cruzi* CYP51, while (*S*)-**1** is more linear (Figure 2D). The different binding modes of (*S*)-**1** and (*R*)-**2** affect the conformations of interacting amino acid residues, thus changing the landscape of the CYP51 binding site for the two compounds. The entrance from the solvent-accessible area remains quite open when (*S*)-**1** is bound,

partially due to flexibility of the M460 side chain (which is not resolved in the X-ray structure of *T. brucei* CYP51 complexed with (*S*)-**1**) (Figure 1B). When (*R*)-**2** is bound, the interactions between M460 and the central phenyl ring of the inhibitor are established and partially block the entrance to the active site (Figure 2C).

On the basis of the *Tc*CYP51-(*R*)-**2** cocrystal structure, 17 hydrophobic amino acid residues, F48, Y103, I105, M106, F110, Y116, P210, V213, F214, A287, F290, A291, T295, L356, M358, M360, M460, and V461, constitute the binding site within 5 Å of (*R*)-**2** (Figure 3). No direct H-bonds between (*R*)-**2** and the *Tc*CYP51 target are suggested by the cocrystal structure, with the qualification that water molecules, which might potentially mediate such contacts, may not be resolved at 3.1 Å. The amino acids I45, F48, I72, V213, L357, M358, and M360 surround the terminal 3-fluorophenyl ring of (*R*)-**2** (Figure 3), providing space to explore a variety of ring substituents. By applying structure-based molecular design considerations,^{21,22} a series of (*R*)-**2** analogues were synthesized with the objective to increase potency against *T. cruzi*. Specifically, additional substituents on the terminal phenyl ring were introduced to fill the hydrophobic pocket identified in the cocrystal structure. In addition, a flexible piperazine ring was inserted between the aromatic rings of the rigid biaryl unit to probe binding interactions in the hydrophobic pocket projecting toward the solvent accessible area. A diverse set of new inhibitors was synthesized, among which (*R*)-**3**–(*R*)-**8** (see Scheme 1 for syntheses of these compounds) are particularly potent (Table 1). The (*S*)-enantiomers of several of these and of other inhibitors were also synthesized and in all cases were found to be considerably less potent than the corresponding (*R*)-enantiomers (see Table S1 and Figure S2, Supporting Information).

The 3,4-difluoro analogue (*R*)-**4** gained an order of magnitude in potency compared to (*R*)-**2**, while potency of the 2,5-analogue (*R*)-**3** dropped an order of magnitude. The potency gain by (*R*)-**4** is likely due to hydrophobic interactions between the 4-fluoro substituent and the side chain of F48 (Figure 3), which is otherwise missing from the electron density. Increasing the size of the substituent from 4-fluoro in (*R*)-**4** to 4-trifluoromethyl in (*R*)-**5** resulted in a ca. 600-fold loss in potency, while its microsomes stability and selectivity to human CYP enzymes were significantly improved compared to (*R*)-**4**. Insertion of a piperazine ring between the aryl groups yielded (*R*)-**6**, which was only 4-fold less potent than (*R*)-**2**. Both (*R*)-**7** and (*R*)-**8** with terminal fluorine-substituted benzyl ethers maintained EC₅₀ potency comparable to (*R*)-**2** and (*R*)-**5**, respectively. Two of these compounds, (*R*)-**5** and (*R*)-**8**, had substantially improved microsomes stability compared to (*R*)-**2**, and (*R*)-**8** in particular had a substantially improved inhibition profile vs human CYP enzymes (Table 1). The binding poses of inhibitors were predicted by docking studies using Glide (see Figure S3, Supporting Information, for details). The terminal phenyl ring of (*R*)-**6** fits well into the hydrophobic pocket near to the biaryl ring of (*R*)-**2**. In addition, the benzyl moiety of (*R*)-**7** or (*R*)-**8** is oriented toward the solvent accessible area or the hydrophobic pocket, respectively.

In summary, a new series of 4-pyridinyl-based CYP51 inhibitors has been developed by using structure-guided molecular design methodology. Starting with the cocrystal structure of (*S*)-**1** bound to *T. brucei* CYP51, we significantly improved inhibitor potency by switching to the *R*-configuration of the inhibitor scaffold. Compared to the *S*-enantiomer series,

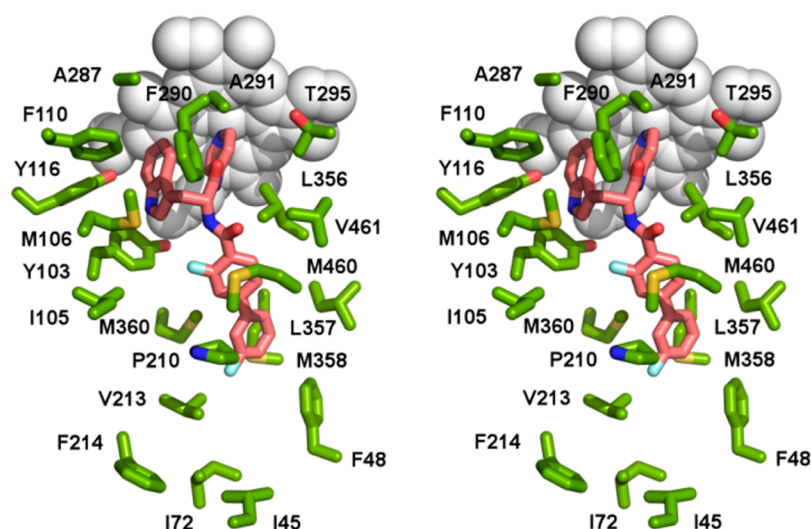


Figure 3. Stereogram of the (*R*)-2 binding site in *TcCYP51*. Amino acid residues (green) are shown within 5 Å of (*R*)-2 (red), plus those constituting a cavity surrounding the terminal 3-fluorophenyl ring of (*R*)-2. The side chains of I45 and F48, disordered in the X-ray structure, are reconstituted by molecular modeling. Heme is in gray spheres.

the antiparasite efficacy of some *R*-inhibitor isomers increased >1000-fold in the cell-based assay, with concomitant increases in microsome stability and selectivity against human drug metabolizing CYPs. The cocrystal structure of (*R*)-2 with the ultimate therapeutic target, *T. cruzi* CYP51, aided in the design of the next generation of inhibitor analogues, one of which (*R*)-4 is a ca. 20 pM inhibitor of *T. cruzi* in cell culture, while the less potent analogue (*R*)-8 has excellent in vitro PK properties. Collectively, this work demonstrates that the *R*-series of *N*-indolyl-oxopyridinyl-4-aminopropanyl inhibitors has considerable promise for the development of anti-*T. cruzi* therapeutics. Further studies toward this goal will be reported in due course.

■ ASSOCIATED CONTENT

■ Supporting Information

Experimental procedures for *T. cruzi* cell-based assay, X-ray structure analysis, hepatic microsome stability and CYP inhibition assays, chemical synthesis of the inhibitors, and the dose–response curves and binding poses of the compounds predicted by molecular docking. This material is available free of charge via the Internet at <http://pubs.acs.org>.

Accession Codes

The atomic coordinates and structure factors (PDB ID codes 4BY0) have been deposited in the Protein Data Bank, Research Collaboratory for Structural Bioinformatics, Rutgers University, New Brunswick, NJ (<http://www.rcsb.org/>).

■ AUTHOR INFORMATION

Corresponding Authors

*(W.R.R.) E-mail: roush@scripps.edu.

*(L.M.P.) E-mail: larissa.podust@ucsf.edu.

Present Address

#College of Science and Engineering, Seattle University, Seattle, Washington 98122, United States

Author Contributions

The manuscript was written through contributions of all authors. All authors have given approval to the final version of the manuscript.

Funding

This research was generously supported by NIH R01 grant AI095437, and C.M.C was supported by Conselho Nacional de Desenvolvimento Científico e Tecnológico (CNPq) and FIOCRUZ, Brazil. The Advanced Light Source is supported by the Director, Office of Science, Office of Basic Energy Sciences, of the U.S. Department of Energy under Contract No. DE-AC02-05SCH11231.

Notes

The authors declare no competing financial interest.

■ ACKNOWLEDGMENTS

We thank the staff members of beamline 8.3.1, James Holton, George Meigs, and Jane Tanamachi, at the Advanced Light Source at Lawrence Berkeley National Laboratory, for assistance with data collection, Claudia Ruiz (Scripps Florida) for microsome stability assays, and Potter Wickware for proof reading of the manuscript.

■ ABBREVIATIONS

T. cruzi, *Trypanosoma cruzi*; CYP51, cytochrome P450 isoform 51; EC₅₀, half-maximal effective concentration

■ REFERENCES

- (1) Becher, R.; Wirsal, S. G. Fungal cytochrome P450 sterol 14 α -demethylase (CYP51) and azole resistance in plant and human pathogens. *Appl. Microbiol. Biotechnol.* **2012**, *95*, 825–840.
- (2) Kathiravan, M. K.; Salake, A. B.; Chothe, A. S.; Dudhe, P. B.; Watode, R. P.; Mukta, M. S.; Gadhwane, S. The biology and chemistry of antifungal agents: a review. *Bioorg. Med. Chem.* **2012**, *20*, S678–S698.
- (3) Buckner, F. S.; Urbina, J. A. Recent developments in sterol 14-demethylase inhibitors for Chagas disease. *Int. J. Parasitol. Drugs Drug Resist.* **2012**, *2*, 236–242.
- (4) Diniz Lde, F.; Caldas, I. S.; Guedes, P. M.; Crepalde, G.; de Lana, M.; Carneiro, C. M.; Talvani, A.; Urbina, J. A.; Bahia, M. T. Effects of ravuconazole treatment on parasite load and immune response in dogs experimentally infected with *Trypanosoma cruzi*. *Antimicrob. Agents Chemother.* **2010**, *54*, 2979–2986.
- (5) Molina, J.; Martins-Filho, O.; Brener, Z.; Romanha, A. J.; Loebenberg, D.; Urbina, J. A. Activities of the triazole derivative SCH 56592 (posaconazole) against drug-resistant strains of the protozoan parasite *Trypanosoma* (*Schizotrypanum*) *cruzi* in immunocompetent

and immunosuppressed murine hosts. *Antimicrob. Agents Chemother.* **2000**, *44*, 150–155.

(6) Kraus, J. M.; Tatipaka, H. B.; McGuffin, S. A.; Chennamaneni, N. K.; Karimi, M.; Arif, J.; Verlinde, C. L.; Buckner, F. S.; Gelb, M. H. Second generation analogues of the cancer drug clinical candidate tipifarnib for anti-Chagas disease drug discovery. *J. Med. Chem.* **2010**, *53*, 3887–3898.

(7) Andriani, G.; Amata, E.; Beatty, J.; Clements, Z.; Coffey, B. J.; Courtemanche, G.; Devine, W.; Erath, J.; Juda, C. E.; Wawrzak, Z.; Wood, J. T.; Lepesheva, G. I.; Rodriguez, A.; Pollastri, M. P. Antitrypanosomal lead discovery: Identification of a ligand-efficient inhibitor of *Trypanosoma cruzi* CYP51 and parasite growth. *J. Med. Chem.* **2013**, *56*, 2556–2567.

(8) Villalta, F.; Dobish, M. C.; Nde, P. N.; Kleshchenko, Y. Y.; Hargrove, T. Y.; Johnson, C. A.; Waterman, M. R.; Johnston, J. N.; Lepesheva, G. I. VNI cures acute and chronic experimental Chagas disease. *J. Infect. Dis.* **2013**, *208*, 504–511.

(9) Buckner, F. S.; Wilson, A. J.; White, T. C.; Van Voorhis, W. C. Induction of resistance to azole drugs in *Trypanosoma cruzi*. *Antimicrob. Agents Chemother.* **1998**, *42*, 3245–3250.

(10) Choi, J. Y.; Calvet, C. M.; Gunatilleke, S. S.; Ruiz, C.; Cameron, M. D.; McKerrow, J. H.; Podust, L. M.; Roush, W. R. Rational development of 4-aminopyridyl-based inhibitors targeting *Trypanosoma cruzi* CYP51 as anti-Chagas agents. *J. Med. Chem.* **2013**, *56*, 7651–7668.

(11) Chen, C.-K.; Doyle, P. S.; Yermalitskaya, L. V.; Mackey, Z. B.; Ang, K. K. H.; McKerrow, J. H.; Podust, L. M. *Trypanosoma cruzi* CYP51 inhibitor derived from a *Mycobacterium tuberculosis* screen hit. *PLoS Negl. Trop. Dis.* **2009**, *3*, e372.

(12) Chen, C.-K.; Leung, S. S. F.; Guilbert, C.; Jacobson, M. P.; McKerrow, J. H.; Podust, L. M. Structural characterization of CYP51 from *Trypanosoma cruzi* and *Trypanosoma brucei* bound to the antifungal drugs posaconazole and fluconazole. *PLoS Negl. Trop. Dis.* **2010**, *4*, e651.

(13) Arvela, R. K.; Leadbeater, N. E. Suzuki coupling of aryl chlorides with phenylboronic acid in water, using microwave heating with simultaneous cooling. *Org. Lett.* **2005**, *7*, 2101–2104.

(14) Barder, T. E.; Walker, S. D.; Martinelli, J. R.; Buchwald, S. L. Catalysts for Suzuki–Miyaura coupling processes: scope and studies of the effect of ligand structure. *J. Am. Chem. Soc.* **2005**, *127*, 4685–4696.

(15) Kudo, N.; Perseghini, M.; Fu, G. C. A versatile method for Suzuki cross-coupling reactions of nitrogen heterocycles. *Angew. Chem., Int. Ed.* **2006**, *45*, 1282–1284.

(16) Leadbeater, N. E. Fast, easy, clean chemistry by using water as a solvent and microwave heating: the Suzuki coupling as an illustration. *Chem. Commun.* **2005**, 2881–2902.

(17) Tasler, S.; Mies, J.; Langa, M. Applicability aspects of transition metal-catalyzed aromatic amination protocols in medicinal chemistry. *Adv. Synth. Catal.* **2007**, *349*, 2286–2300.

(18) Wolfe, J. P.; Buchwald, S. L. Improved functional group compatibility in the palladium-catalyzed amination of aryl bromides. *Tetrahedron Lett.* **1997**, *38*, 6359–6362.

(19) Wolfe, J. P.; Buchwald, S. L. Scope and limitations of the Pd/BINAP-catalyzed amination of aryl bromides. *J. Org. Chem.* **2000**, *65*, 1144–1157.

(20) Coste, J.; Lenguyen, D.; Castro, B. Pybop: a new peptide coupling reagent devoid of toxic by-product. *Tetrahedron Lett.* **1990**, *31*, 205–208.

(21) Greer, J.; Erickson, J. W.; Baldwin, J. J.; Varney, M. D. Application of the three-dimensional structures of protein target molecules in structure-based drug design. *J. Med. Chem.* **1994**, *37*, 1035–1054.

(22) Kuntz, I. D. Structure-based strategies for drug design and discovery. *Science* **1992**, *257*, 1078–1082.